Int. J. Appl. Comput. Math (2025) 11:151
https://doi.org/10.1007/s40819-025-01973-z

ORIGINAL PAPER

Numerical Investigation of Heat Transfer Performance of Hybrid Nanofluid in Porous Substrate in Microchannel Heat Sink

Jeremiah O. Oladetan[1] · Faridat M. Fujah[1] · Oluwasegun S. Omosehin[1,2] · Emmanuel O. Atofarati[3] · Uzo Nwabuko[1] · Olabode T. Olakoyejo[1,4] · Adekunle O. Adelaja[4]

Received: 15 October 2024 / Accepted: 8 July 2025 / Published online: 29 July 2025
© The Author(s) 2025

Abstract
With the increasing integration of integrated circuits (ICs) in electronic devices such as electric vehicles, computer data centers, heat pipe technology, solar energy, and heating ventilation, air conditioning, and refrigeration (HVACR) systems, optimizing heat transfer becomes essential to ensure optimal performance and longevity. This study numerically investigates the thermal and hydraulic performance of a microchannel heat sink (MCHS) enhanced by hybrid nanofluids and porous substrate integration. A two-phase Eulerian–Eulerian model implemented in ANSYS Fluent is employed to simulate Al_2O_3/Cu–water hybrid nanofluid flow at volume concentrations ranging from 0.1 to 3.0%, and flow Reynolds number ($200 < Re < 1000$) with a porous substrate embedded midway along the flow path. The results reveal that both the nanoparticle concentration and Reynolds number significantly enhance heat transfer, reflected in higher average Nusselt numbers and reduced thermal resistance. The incorporation of a porous substrate further amplifies heat transfer, achieving a maximum enhancement of 80.29% compared to the baseline configuration. Overall, employing hybrid nanofluids and porous substrates improves MCHS performance, offering augmented heat transfer efficiency and thermal performance.

✉ Oluwasegun S. Omosehin
omosehin.os@up.ac.za

✉ Emmanuel O. Atofarati
atofae@unisa.ac.za

1 Department of Aerospace Engineering, Lagos State University, Epe Campus, Lagos, Nigeria

2 Department of Mechanical and Aeronautical Engineering, University of Pretoria, Pretoria, Private Bag X20, Hatfield 0028, South Africa

3 Department of Mechanical, Bioresources and Biomedical Engineering, University of South Africa, Science Campus, Johannesburg 1710, FL, South Africa

4 Department of Mechanical Engineering, University of Lagos, Akoka, Yaba, Lagos 101017, Nigeria

Keywords Microchannel · Hybrid nanofluid · Porous substrate · Convective heat transfer · Heat sink

Abbreviations

A	Area (m^2)
C	Forchheimer's constant
C_p	Specific heat capacity (J/KgK)
Cu	Copper
C_d	Drag coefficient (---)
D_h	Hydraulic diameter (m)
F_D	Drag force (Pa/m)
F_{VM}	Virtual mass (Pa/m)
F_{Col}	Particle-Particle interaction force (Pa/m)
H_{ch}	Channel height (μm)
H_p	Porous media height (μm)
k	Thermal conductivity (W/m.K)
K	Permeability of porous substrate (m^2)
L	Length (μm)
L_p	Porous media length
Nu	Nusselt number (---)
P	Pressure (Pa)
PM	Porous media/substrate
ΔP	Pressure-drop (KPa)
q^{ii}	Heat flux (W/m^2)
Q_h	Volumetric rate of energy transfer (J/m^3 s)
Re	Reynolds number (---)
R_{th}	Thermal resistance (K/W)
T	Temperature (K)
$\vec{V}$	Velocity vector (m/s)
W_{ch}	Channel width (μm)
W_p	Porous media width
Δ	Difference
P	Density (kg/m^3)
α	Volume concentration (--)
μ	Dynamic viscosity (kg/m s)
γ	porosity
β	Friction coefficient (kg/m^3 s)
Φ	Form factor
Avg	Average
B	base
B	Bulk
I	Inlet
P	Particle
S	Solid
f	Fluid
w	Wall

1	Primary phase (Water)
2	Secondary phase (Alumina particles)
3	Secondary phase (Copper particles)

Introduction

In the realm of thermal management, the synergy between integrated circuits (ICs), micro-electromechanical systems (MEMS), and advanced micro-cooling technologies for electronic devices drives a relentless pursuit of enhanced heat transfer efficiency. Conventional fluids like air, water, glycol, ethylene, mineral oil, and engine oil are inadequate for the escalating thermal demands of modern devices [1–3]. As electronic devices become more sophisticated and compact, the challenge of dissipating the heat generated becomes paramount to ensure the reliability and durability of the devices [4].

This necessitates a shift towards nanofluids, integrating nanoparticles into carrier fluids, offering transformative heat transfer enhancement. Pioneered by Choi and Eastman [5], nanofluids promise unprecedented performance across diverse applications, heralding improved efficiency and innovation in heat management. Other studies have shown the advances of nanofluid for heat transfer applications [6, 7]. Microchannels consist of intricately arranged tunnel-like structures or walls embedded within the heat transfer substrate to improve device cooling. These microstructures' walls increase the available surface area for effective heat transfer. Within these channels, a cooling fluid, often water, flows, aiding the transfer of heat energy from the walls through conduction and convection processes. High heat transfer coefficients, compact size, and low-pressure drop defining characteristics of micro-channel heat sinks (MCHSs) position them as a promising technology for cooling high heat flux electrical devices [8, 9].

Researchers have rigorously analyzed MCHSs with nanofluids, exploring experimental, numerical, and mathematical methodologies to optimize heat transfer efficiency [9–11]. Gupta and Subbarao [9] experimentally and numerically studied the behavior of an Al_2O_3-water nanofluid in MCHS at low flow Reynolds numbers in the range of 10–50. The results demonstrate that the nanofluid effectively reduced the average surface temperature in the MCHS and enhanced the heat transfer rate by approximately 43%. Notably, a nanofluid concentration of 4% wt. exhibited the most favorable heat transfer performance, while a concentration of 3% wt. yielded optimal thermo-hydraulic performance.

Najafpour et al. [10], conducted a numerical analysis to assess the hydrothermal behavior of various cross-sectional geometries of MCHS, employing TiO_2/MgO/GO-water trihybrid nanofluids as the heat transfer medium. Their findings indicate that MCHS with a trapezoidal cross-section exhibited superior thermal performance, while those with a rhombus cross-section demonstrated the most favorable temperature distribution. Moreover, the study revealed a direct correlation between thermal performance and the concentration of the trihybrid nanofluid, with the nanofluid containing 0.05 vol% exhibiting the highest heat transfer coefficient. Jing et al. [12] also investigated the cooling capacity of elliptical microchannels of different sizes. Additionally, they observed that in microchannels with smaller hydraulic diameters, slip exerts a more pronounced influence, attenuating hydraulic resistance while enhancing heat transfer.

The optimization of micro-cooling channels for effective thermal management in heat-generating systems has seen significant advancements through various studies. Olakoyejo et al. [13] applied constructal theory to optimize three-dimensional cylindrical micro-cooling channels, focusing on variable cross-section configurations. Their aim was to minimize thermal resistance and friction factor while enhancing cooling performance using water as the coolant. This study employed ANSYS FLUENT to identify optimal inlet and outlet diameters, showing significant improvements in the system's thermal efficiency. In a related investigation, Olakoyejo et al. [14] examined an elliptical microchannel heat sink with Al_2O_3-water nanofluid, revealing that higher aspect ratios, nanoparticle concentrations, and Reynolds numbers enhance heat transfer efficiency and reduce entropy generation. Similarly, Olakoyejo et al. [15] conducted a numerical analysis on diamond-hole cooling channels, demonstrating that optimal aspect ratios and Reynolds numbers decrease maximum temperature and thermal resistance while improving the Nusselt number. These studies collectively underscore the importance of channel design and fluid properties in optimizing the thermal performance of micro-cooling systems.

Sheik et al. [11] investigated the impact of open and closed triangular-finned MCHS configurations utilizing SiO_2 nanofluids at Reynolds numbers in the range of 200 to 800, with varying fin heights from 0.5 mm to 2.0 mm. Their study revealed that at an optimal fin height of 1.0 mm, the utilization of SiO_2 nanofluid led to a remarkable enhancement in thermal performance, with a 58% increase in thermal performance factor compared to water. Martinez et al. [16] also investigated the impact of flow rate and microchannel height. Additionally, they found that both the utilization of nanofluids and the reduction of microchannel height promote heat transfer at low Reynolds numbers. However, they observed that the efficacy of these improvements diminishes as the Reynolds number increases.

Kalteh et al. [17] conducted an in-depth investigation into laminar convective heat transfer phenomena within a wide rectangular microchannel heat sink, utilizing an alumina-water based nanofluid. Employing a combination of experimental validation and numerical simulations, they discerned that the two-phase modeling approach exhibited superior agreement with experimental data compared to the homogeneous (single-phase) modeling. Their finding elucidates the heightened appropriateness of employing the two-phase method for accurately simulating nanofluid heat transfer dynamics within microchannel configurations. Omosehin et al. [18], analyzed the thermal behavior and pressure loss of water-based Cu- Al_2O_3 hybrid nanofluids in a microchannel heat sink (MCHS). They investigated the impact of alumina and copper hybridization on bulk and substrate temperatures, Nusselt number, thermal resistance, and pressure loss across various Reynolds numbers. The study concluded that increasing copper nanoparticle concentration reduced thermal resistance and temperatures but raised the pressure loss, Nusselt number, and figure of merit (FOM).

Rikitu and Makinde [19] conducted a numerical investigation into the mixed convective heat transfer characteristics of a microchannel filled with porous media, utilizing Cu/water nanofluids as the working fluid. They modeled the porous media using the Darcy–Forchheimer approach. Their findings demonstrated that the heat transfer rate within the microchannel increased in direct correlation with the flow Reynolds number, Darcy number, Eckert number, Grashof number, and the viscosity parameter. Similarly, Jalili et al. [20] investigated the impact of a magnetic field on heat transfer in a microchannel filled with porous media using Al_2O_3/water nanofluid. They employed the Koo–Kleinstreuer model to simulate the thermophysical properties of the nanofluid and an enhanced Darcy relationship for the porous media, considering factors such as fluid velocity, nanoparticle diameter and void fraction, channel geometry, temperature distribution, and Hartmann number. Their results indicated a direct correlation between the magnetic field and the Nusselt number, revealing that heat transfer efficiency increased with higher nanofluid concentration.

Additionally, Abdollahi et al. [21] performed a numerical study on the thermal performance of a microchannel filled with porous media using Cu-Al_2OOH/water hybrid nanofluid. Their findings showed that the thermal conductivity of the fluid improved due to the Brownian motion of particles and the porosity of the media. Similar research conducted by Adio et al. [22], Farahani et al. [23, 24], and Wang et al. [25] further highlights the importance of understanding the effects of hybrid nanofluids and porous media on heat transfer with minimal pressure drop. Such studies are crucial for optimizing energy removal in electronic devices and enhancing energy collection in solar thermal systems.

Recent advances in microchannel heat sink (MCHS) technology have highlighted the promise of hybrid nanofluids for enhancing thermal transport due to their tunable thermophysical properties and superior heat dissipation characteristics [26, 27]. While single-phase models have often been applied in early studies, their inability to capture the dynamic interactions between dispersed nanoparticles and base fluids limits their accuracy, especially under varying volume fractions and flow regimes. In response to these limitations, the two-phase Eulerian–Eulerian model has emerged as a robust numerical approach, enabling independent treatment of both the solid and liquid phases [28]. For instance, Gorjaei and Rahmani [29] employed the Eulerian–Eulerian model to investigate forced convection of SiO_2–ethylene glycol nanofluid under single and twin jet injection scenarios in a 2D channel. Their work demonstrated that nanoparticle concentration and jet configuration significantly affected the local Nusselt number, entropy generation, and Darcy friction factor, effects which were better captured through the Eulerian–Eulerian framework compared to conventional single-phase modeling.

Building on this, Bazdidi-Tehrani et al. [30] explored the laminar forced convection of a novel Al_2O_3–n-octadecane/water hybrid nanofluid, where n-octadecane acted as a nano-encapsulated phase change material (NEPCM), through a square microchannel. Their comparative analysis of single-phase and Eulerian–Eulerian approaches revealed that the Eulerian–Eulerian model provided a more accurate depiction of local heat transfer enhancement, thermal development delay, and nanoparticle dispersion behavior, especially at higher nanoparticle volume fractions and Reynolds numbers. Notably, the Eulerian–Eulerian model predicted a maximum gain in total efficiency of up to 60%, compared to 27% for the single-phase model, underscoring the necessity of a multiphase framework in capturing the synergistic thermal contributions of complex nanoparticle blends like NEPCM–metal oxide hybrids.

In a more recent study, Olakoyejo et al. [31] applied the Eulerian–Eulerian model to simulate the thermal-hydraulic and entropy generation characteristics of Al_2O_3–Cu/water hybrid nanofluids in a 3D cylindrical MCHS with internal heat generation. Their results revealed that increases in both copper content and Reynolds number significantly elevated the Nusselt number and suppressed total and thermal entropy generation, with minimal penalties in friction factor. These outcomes not only validated the thermophysical superiority of hybrid nanoparticle suspensions, but also emphasized the Eulerian–Eulerian model's utility in capturing nuanced multiphase flow and energy dissipation phenomena. Collectively, these studies affirm the Eulerian–Eulerian model as a superior computational strategy

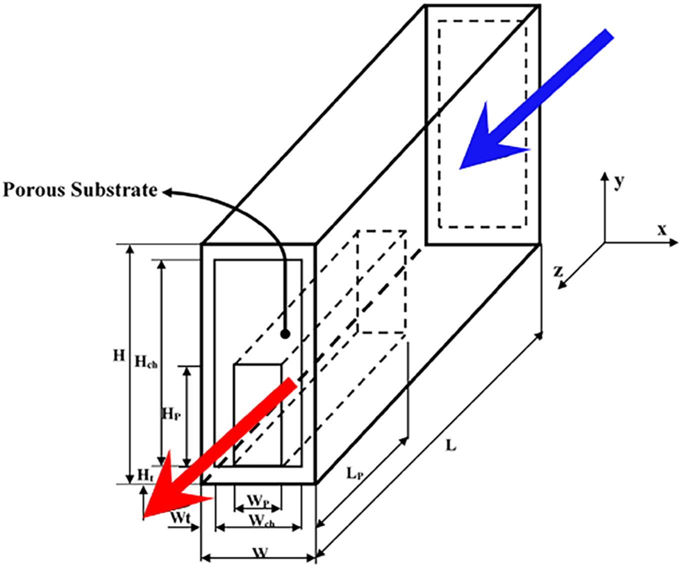

Fig. 1 Geometrical model of the microchannel heat sink with porous substrate

Table 1 Dimensions of the geometrical model

H (µm)	H_{ch}(µm)	H_P(µm)	W (µm)	W_{ch}(µm)	W_P(µm)	L (µm)	L_P (µm)	W_t(µm)	H_t (µm)
1250	1050	525	350	250	150	10,000	5000	50	100

for accurately resolving nanoparticle–fluid interactions in hybrid nanofluid-based thermal systems.

Although numerous studies have explored various strategies to enhance the thermal performance of microchannel heat sinks, there remains a research gap concerning the integrated influence of both hybrid nanofluids and porous substrates within such systems. This study presents a novel investigation into the combined effects of a centrally positioned porous substrate and hybrid nanofluid (Al_2O_3–Cu nanoparticles dispersed in water) on heat transfer and fluid flow in a microchannel heat sink. The performance is analyzed in contrast to four baseline configurations: water only, water with porous substrate, hybrid nanofluid only and hybrid nanofluid with porous substrate. A key innovation of this work lies in modeling the hybrid nanofluid behavior as a two-phase flow using the Eulerian–Eulerian approach. This modeling framework allows for a more physically representative analysis, particularly in non-equilibrium thermal conditions, and offers new insights into the synergistic effects of nanoparticle-fluid dynamics and localized porous media insertion for next-generation thermal management applications.

Numerical Methods and Governing Equation

Details of Model Geometry

The geometrical model presented in Fig. 1 shows a closed, narrow micro-channel heat sink configuration, wherein porous media is strategically positioned centrally and halfway towards the channel outlet, along the side adjacent to the heat source. The geometrical model, along with its vital dimensions outlined in Table 1, embodies both solid and fluid computational zones. The microchannel heat sink (MCHS) is made up of steel block, with a uniform heat flux distribution at the bottom of the micro-channel heat sink. The steel block is considered the computational solid domain, the hybrid nanofluid is the computational fluid region, and the porous substrate is modeled as a special fluid zone to capture flow behavior through the interconnected pores. The hybrid nanofluid, as indicated by the arrow, flows through the microchannel. Table 1 details the geometric dimensions of the setup, including the microchannel height (H_{ch}), porous media height (H_P), channel width (W_{ch}), porous media width (W_P), and channel length (L_{ch}), along with corresponding values in micrometers (μm).

Governing Equations

In this study, we utilize a three-dimensional, laminar, steady-state, and incompressible flow model. To account for the nano particle-fluid interactions and nanoparticle migration which significantly impact thermal performance, the Eulerian-Eulerian two-phase flow model was selected to solve this problem. This model allows for the resolution of separate conservation equations for mass, momentum, and energy for both the base fluid and the nanoparticle phases. Such a framework enables accurate thermal analysis, particularly in regions where temperature gradients or slip velocities between the nanoparticles and the base fluid are significant. It also provides the capability to capture interphase heat and momentum transfer, making it suitable for simulating complex nanofluid behaviors such as particle migration, Brownian motion, and thermophoresis, especially in non-dilute or thermally non-equilibrium conditions [32–34].

The thermophysical properties of the solid phase (nanoparticles) and the conventional/base fluid (pure water) remain temperature-independent throughout the analysis. Ambient conditions are detailed in Table 2. The nanofluid coolant employed in this investigation, namely the Al_2O_3/Cu-water-based hybrid nanofluid, is characterized by a two-phase composition comprising a primary domain/phase (pure water) and two secondary domains (Copper and Alumina particles). Given the focus on flow and heat transfer through a porous substrate within the microchannel heat sink, the mass conservation, momentum, and energy equations are all relevant.

Table 2 Thermo-physical properties of water, copper, and alumina particles

Materials	ρ (kg/m^3)	C_p $(J/kg.K)$	K $(W/m.K)$	μ $(kg/m.s)$
Water	999.1	4184	0.5769	0.001003
Alumina particles	3970	765	36	–
Copper particles	8933	385	400	–
Porous substrate: steel	8030	502.48	16.27	–

Mass conservation equation

i. Clear fluid region

The continuity equations of the clear fluid region of the base fluid and nanoparticles are presented as follows:

Primary phase (Water).

$$\nabla . \left(\alpha_1 \rho_1 \vec{V}_1\right) = 0 \tag{1}$$

Where $\alpha_1,\ \rho_1$, and $\vec{V}_1$ are the volume concentration, density, and velocity vector of the primary domain/phase, respectively.

Secondary phase (Alumina particles).

$$\nabla . \left(\alpha_2 \rho_2 \vec{V}_2\right) = 0 \tag{2}$$

.

Where $\alpha_2,\ \rho_2$, and $\vec{V}_2$ are the volume concentration, density, and velocity vector of the secondary phase (alumina particles), respectively.

Secondary phase (Copper particles).

$$\nabla . \left(\alpha_3 \rho_3 \vec{V}_3\right) = 0 \tag{3}$$

.

Where $\alpha_3,\ \rho_3$, and $\vec{V}_3$ are the volume concentration, density, and velocity vector of the secondary phase (Copper particles), respectively.

ii. Porous region.

The mass conservation equations of the porous region of the base fluid and nanoparticles are presented below.

Primary phase (Water).

$$\nabla . \left(\gamma\, \alpha_1 \rho_1 \vec{V}_1\right) = 0 \tag{4}$$

Secondary phase (Alumina particles).

$$\nabla . \left(\gamma\, \alpha_2 \rho_2 \vec{V}_2\right) = 0 \tag{5}$$

Secondary phase (Copper particles).

$$\nabla . \left(\gamma\, \alpha_3 \rho_3 \vec{V}_3\right) = 0 \tag{6}$$

Where γ represents the Porosity term.

$$\alpha_1 + \alpha_2 + \alpha_3 = 1 \tag{7}$$

The equation for momentum conservation

The equations governing the clear fluid region of both the base fluid and nanoparticles' momentum conservation are outlined in Eqs. (8–11). Within these equations, terms representing the drag force, virtual mass, and particle-to-particle interaction forces (F_{VM}, F_d, and F_{col}, respectively) are accounted for. However, insights from Kalteh et al. [17] suggest that the particle-to-particle interaction forces and virtual mass exhibit negligible influence on heat transfer characteristics, particularly the Nusselt number. As a result, solely the convective heat transfer and frictional drag force between the primary and secondary phases are pertinent. Owing to the diminutive size of the particles, particle-to-particle heat transfer, as well as gravitational and lift forces, are disregarded. The drag force between the primary and each secondary phase (alumina and copper particles) is computed as follows:

i. Clear fluid region.

Primary phase (Water)

$$\nabla.\left(\alpha_1\rho_1\vec{V}_1\vec{V}_1\right) = -\alpha_1.\nabla P + \nabla.\left[\alpha_1\mu_1\left(\nabla.\vec{V}_1 + \nabla.\vec{V}_1^{\,T}\right)\right] + F_d + F_{VM} \tag{8}$$

Secondary phase (Nanoparticles of Alumina)

$$\nabla.\left(\alpha_2\rho_2\vec{V}_2\vec{V}_2\right) = -\alpha_2.\nabla P + \nabla.\left[\alpha_2\mu_2\left(\nabla.\vec{V}_2 + \nabla.\vec{V}_2^{\,T}\right)\right] - F_d - F_{VM} + F_{col} \tag{9}$$

Secondary phase (Nanoparticles of Copper)

$$\nabla.\left(\alpha_3\rho_3\vec{V}_3\vec{V}_3\right) = -\alpha_3.\nabla P + \nabla.\left[\alpha_3\mu_3\left(\nabla.\vec{V}_3 + \nabla.\vec{V}_3^{\,T}\right)\right] - F_d - F_{VM} + F_{col} \tag{10}$$

$$F_d = -\beta.\left(\vec{V}_1 - \vec{V}_p\right) \tag{11}$$

The drag force coefficient by Rowe and Henwood [35, 36] and Wen [37] is given as.

$$\beta = \frac{3}{4}C_d\frac{\alpha_1\alpha_p}{\phi_p d_p}\rho_1\left|\vec{V}_1 - \vec{V}_p\right|\alpha_1^{-2.65} \text{ Applicable for two-phase flow } \alpha_1 > 0.8 \tag{12}$$

Applicable for two-phase flow $\alpha_1 > 0.8$ (12)

ϕ_p the form factor is taken as one for a spherical particle.

$$C_d = \begin{cases} \frac{24}{Re_p}\left(1 + 0.15{Re_p}^{0.687}\right) Re_p < 1000 \\ 0.44 Re_p \geq 1000 \end{cases} \tag{13}$$

Where:

$$Re_p = \frac{\alpha_1 \rho_1 \left| \vec{V}_1 - \vec{V}_p \right| d_p}{\mu_1} \tag{14}$$

The equivalences are established as follows $\vec{V}_p$, α_p, and Re_p correspond to $\vec{V}_2$, α_2, and Re_2 for the secondary phase comprising alumina particles, while $\vec{V}_p$, α_p, and Re_pcorrespond to $\vec{V}_3$, α_3, and $Re_3$for the secondary phase consisting of copper particles. Moreover, both alumina and copper particles possess similar particle diameter (d_p) of 40 nm.

ii. Porous region.

The momentum conservation equation for the porous region, encompassing the base fluid (water) and nanoparticles, is obtainable as follows.

Primary phase (Water)

$$\nabla.\left(\gamma\alpha_1\rho_1\vec{V}_1\vec{V}_1\right) = -\gamma\alpha_1.\nabla P + \nabla.\left[\gamma\alpha_1\ \mu_1\ \left(\nabla.\vec{V}_1 + \nabla.\vec{V}_1^T\right)\right] + \gamma F_d + \gamma F_{VM} + \alpha_1\left(\frac{\mu}{K} + \frac{C\rho_1\vec{V}_1}{\sqrt{K}}\right)\vec{V}_1 \tag{15}$$

Secondary phase (Alumina particles)

$$\nabla.\left(\gamma\alpha_2\rho_2\vec{V}_2\vec{V}_2\right) = -\gamma\alpha_2.\nabla P + \nabla.\left[\gamma\alpha_2\ \mu_2\ \left(\nabla.\vec{V}_2 + \nabla.\vec{V}_2^T\right)\right] + \gamma F_d + \gamma F_{VM} + \alpha_2\left(\frac{\mu}{K} + \frac{C\rho_2\vec{V}_2}{\sqrt{K}}\right)\vec{V}_2 \tag{16}$$

Secondary phase (Copper particles)

$$\nabla.\left(\gamma\alpha_3\rho_3\vec{V}_3\vec{V}_3\right) = -\gamma\alpha_3.\nabla P + \nabla.\left[\gamma\alpha_3\ \mu_3\ \left(\nabla.\vec{V}_3 + \nabla.\vec{V}_3^T\right)\right] + \gamma F_d + \gamma F_{VM} + \alpha_3\left(\frac{\mu}{K} + \frac{C\rho_3\vec{V}_3}{\sqrt{K}}\right)\vec{V}_3 \tag{17}$$

$$C = \frac{1.75}{\sqrt{150}\,\gamma^{3/2}} \tag{18}$$

$$K = \frac{{d_p}^2\,\gamma^3}{175\,(1-\gamma)^2} \tag{19}$$

Where, $\gamma = 0.65$,

Energy conservation equation

i. Clear fluid region.

The energy conservation equation for the clear fluid zone of both the base fluid and nanoparticles, neglecting contributions from viscous dissipation and radiation, is presented below.

Primary phase (Water)

$$\nabla.\left(\alpha_1\rho_1\vec{V}_1 C_{p_1} T_1\right) = \nabla.\left(\alpha_1 k_1 \nabla T_1\right) - Q_h \tag{20}$$

Secondary phase (Alumina particles)

$$\nabla . \left(\alpha_2 \rho_2 \overrightarrow{V}_2 C_{p_2} T_2\right) = \nabla . (\alpha_2 k_2 \nabla T_2) - Q_h \tag{21}$$

Secondary phase (Copper particles)

$$\nabla . \left(\alpha_3 \rho_3 \overrightarrow{V}_3 C_{p_3} T_3\right) = \nabla . (\alpha_3 k_3 \nabla T_3) - Q_h \tag{22}$$

Where,

Q_h the volumetric rate of heat transfer between the primary and each secondary phase (copper and alumina nanoparticles).

$$Q_h = \alpha_1 h_{p_1} (T_p - T_1) \tag{23}$$

ii. Porous region.

The energy conservation equation for the porous region containing both the base fluid (i.e., water) and nanoparticles (i.e., alumina and copper), with viscous dissipation and radiation neglected, is provided below.

Primary phase (Water)

$$\nabla . \left(\gamma \alpha_1 \rho_1 \overrightarrow{V}_1 C_{p_1} T_1\right) = \nabla . (\gamma \alpha_1 k_1 \nabla T_1) - Q_h \tag{24}$$

Secondary phase (Alumina nanoparticles)

$$\nabla . \left(\gamma \alpha_2 \rho_2 \overrightarrow{V}_2 C_{p_2} T_2\right) = \nabla . (\gamma \alpha_2 k_2 \nabla T_2) - Q_h \tag{25}$$

Secondary phase (Copper nanoparticles)

$$\nabla . \left(\gamma \alpha_3 \rho_3 \overrightarrow{V}_3 C_{p_3} T_3\right) = \nabla . (\gamma \alpha_3 k_3 \nabla T_3) - Q_h \tag{26}$$

$$Q_h = (1 - \gamma) \alpha_1 h_{p_1} (T_p - T_1) \tag{27}$$

Such that h_{p_1} and T_p corresponds to h_{21} and T_2 for the alumina nanoparticles

h_{p_1} and T_p corresponds to h_{31} and T_3 for the copper nanoparticles

h_{p_1} is calculated from the Gunn model as the fluid-particle convective heat transfer coefficient [18, 38].

Solid wall domain's Energy equation

The transfer of heat in the solid wall was represented by

$$k_s \nabla^2 T_s = 0 \tag{28}$$

Thermal Boundary Conditions

The channel introduces the particulate phase and base fluid with equal axial velocity and at an initial temperature of 25°C. The Solid boundaries enforce a no-slip condition, as indicated in the previous study by Omosehin et al. [18] and Schlichting and Gersten [39]. An outflow condition is applied at the channel outlet, assuming a fully developed flow for comparison with experiments. The thermal boundary conditions include adiabatic boundaries for the solid domain, except for the bottom of the microchannel, where a fixed heat flux of 1 MW/m² is utilized, as depicted in Fig. 2. Mathematical expressions for these conditions follow.

Inlet conditions

$$T_f = T_{in} = 25^oC \ for\, z = 0, \ W_t \le x \le W_t + W_{ch} \ and \ H_t \le y \le H_t + H_{ch} \tag{29}$$

$V_f = V_{in}$ (uniform axial velocity of nanofluid) (30)

Outlet conditions

Outflow condition was applied at the outlet.

$$\frac{\partial^2 T_f}{\partial X^2} = 0 \, for\, z = L, \ W_t \le x \le W_t + W_{ch} \ and \ H_t \le y \le H_t + H_{ch} \tag{31}$$

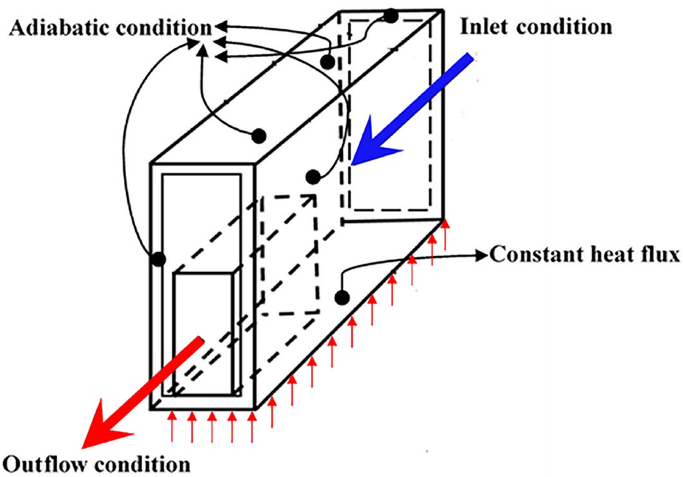

Fig. 2 Boundary conditions around the geometrical model

Channel bottom (constant heat flux)

$$-k_s \frac{\partial T_s}{\partial Z} = q'' \quad for\, 0 \leq z \leq L,\; 0 \leq x \leq W \quad and\, y = 0 \tag{32}$$

Interface condition

$$T_s = T_f \tag{33}$$

$$-k_s \frac{T_s}{\partial n} = -k_f \frac{T_f}{\partial n} \tag{34}$$

Where k_f is the thermal conductivity of the fluid.

Pressure-Drop across the Microchannel

The pressure drop within the micro-channel was determined by subtracting the downstream pressure from the upstream pressure. These pressures denoted as P_{out} and P_{in}, respectively, represent the mean-weighted average pressures at the outlet and inlet, derived from numerical simulations conducted in the ANSYS Postprocessor. As a result, the pressure-loss (ΔP) within the entire microchannel is calculated as,

$$\Delta P = P_{in} - P_{out} \tag{35}$$

Average Nusselt Number

The average Nusselt number, typically represented as Nu_{avg}serves as a valuable metric when assessing the efficacy of different surfaces and flow conditions in heat transmission. Higher Nusselt numbers indicate more efficient convective heat transfer, while lower values suggest a prevalence of conduction. Nu_{avg} of the flow field hinges on the temperature differential between the mean-wall temperature of the microchannel and the volume-average temperature of the mixture within the channel.

$$Nu_{avg} = \frac{q^{ll}\, D_h}{k_f\, (T_w - T_B)} \tag{36}$$

Where, q'' denotes the wall convective heat flux at the base of the computational domain, and D_h represents the hydraulic diameter of the microchannel (The hydraulic diameter is a standard choice for non-circular and microchannel geometries, and it ensures correct dimensional consistency and meaningful comparison across studies). The liquid's thermal conductivity is denoted as k_f is adopted from prior works presented by Omosehin et al. [18] and Nimmagadda and Venkatasubbaiah [40].

In the Eulerian-Eulerian model, the properties of the mixture phase are calculated as a weighted sum of the properties of each individual phase, with weights based on the phase fractions. Specifically, the thermal conductivity of the mixture is calculated as the sum of the products of the volume fraction and the thermal conductivity of each phase. Where, T_w and T_B represent the area-weighted mean surface (wall) temperature of the microchannel and the volume-weighted average temperature of the mixture obtained after solving the physics in ANSYS postprocessor.

Thermal Resistance

Thermal resistance, a fundamental metric in heat transfer analysis, delineates a material's resistance to heat flow. Within microchannels, it succinctly captures the temperature elevation as fluid traverses. Lowering thermal resistance is imperative for optimal heat dissipation from heat sources. Mathematically presented as

$$R_{th} = \frac{\Delta T}{q^{ii} A_b} \tag{37}$$

$$\Delta \mathrm{T} = T_{max} - T_{in} \tag{38}$$

This parameter, i.e., the base area of the heat sink (A_b), dividing the peak temperature at the heat source ($T_{\max}$), serves as a cornerstone in the design of microchannel heat sinks and other microfluidic devices. It facilitates precise temperature rise forecasts and aids in the calibration of cooling systems. Through the reduction of thermal resistance, the efficacy of microchannel heat sinks and microfluidic devices can be significantly augmented.

Figure of Merit

The Figure of Merit (FOM) is an important indicator in thermal systems because it assesses the overall efficiency of heat transfer improvements relative to the properties of the working fluid. The FOM for the different volume concentrations of the hybrid nanofluid will be calculated. Here, FOM is defined as:

$$FOM = \frac{h_{nf} / h_{bf}}{\left(\rho_{nf} / \rho_{bf} \right)^{1/3}} \tag{39}$$

Where: h_{nf} and h_{bf} represent the convective heat transfer coefficients of the nanofluid and base fluid, respectively.

$\rho_{nf}$and ρ_{bf} are the densities of the nanofluid and base fluid, respectively.

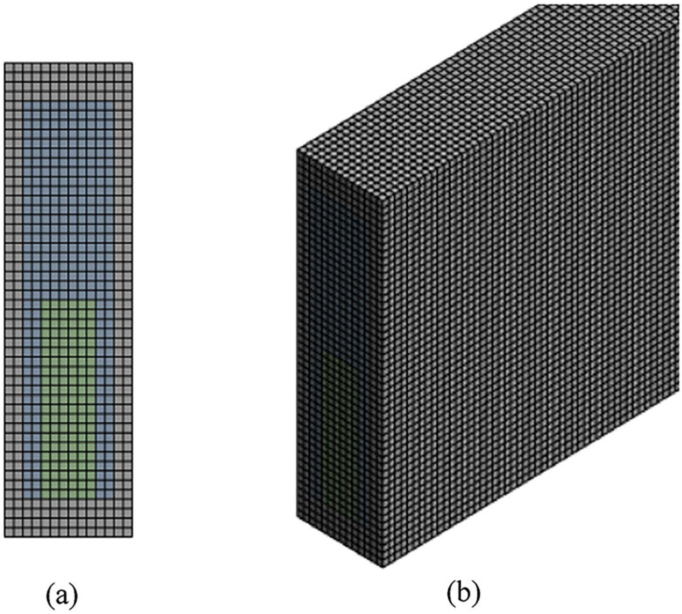

Fig. 3 Mesh independence study of the numerical model

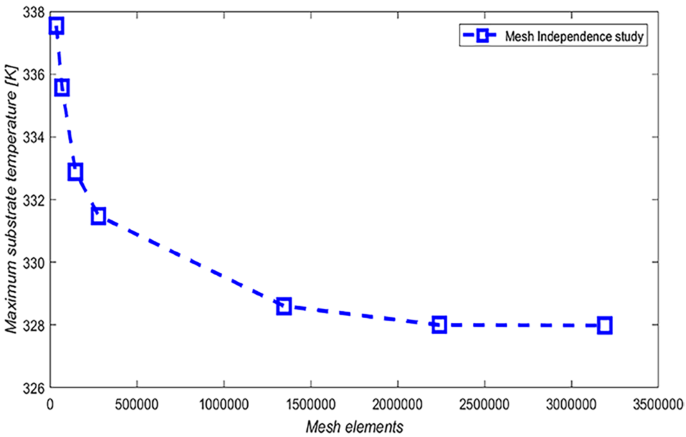

Fig. 4 Mesh generation **a** at the cross-section **b** along the length of the micro channel heat sink

Mesh Independence Study

A mesh independence study is conducted to ensure the result of the numerical model is independent of the number of elements. The base fluid, water is used as the test fluid in the microchannel heat sink integrated with porous substrate and at Reynold number of 400. The study was conducted with different sizes and densities of the elements, from coarse elements of larger size and fewer nodes to extra fine elements of smaller size and more nodes. The peak substrate temperature at the heat source of the microchannel heat sink subjected to a constant heat flux of $1\mathrm{MW/m^2}$ is considered as the test parameter for the study. Figure 3 shows that there is no significant change in the maximum substrate temperature from the very fine mesh to extra fine mesh. Hence, a very fine mesh with about 2.25 million element was selected for further calculations considering computational time and accuracy. An example of the mesh generation is shown in Fig. 4.

Error Analysis

To quantitatively measure the agreements between the numerical results and the experimental results, the mean absolute deviation (MAD) was used as expressed in Eqs. (40).

Mean absolute deviation (MAD):

$$MAD = \frac{1}{n}\sum{}_{1}^{n}\left|\frac{\left(\gamma_{num} - \gamma_{exp}\right) \times 100\%}{\gamma_{exp}}\right| \tag{40}$$

Where, n, is the number of data and γ_{num} and γ_{exp} are the numerical and experimental data such as pressure drop and Nusselt number from which errors are calculated.

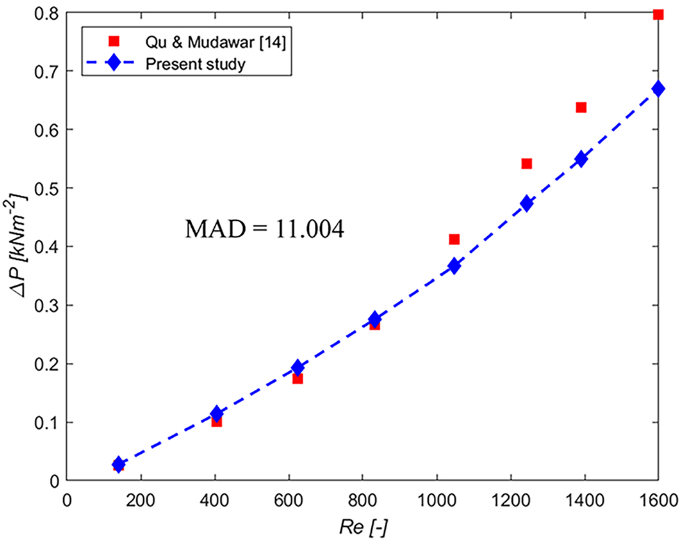

Fig. 5 Comparative analysis of (MCHS without porous medium) pressure drop in present study and Qu and Mudawar [41]

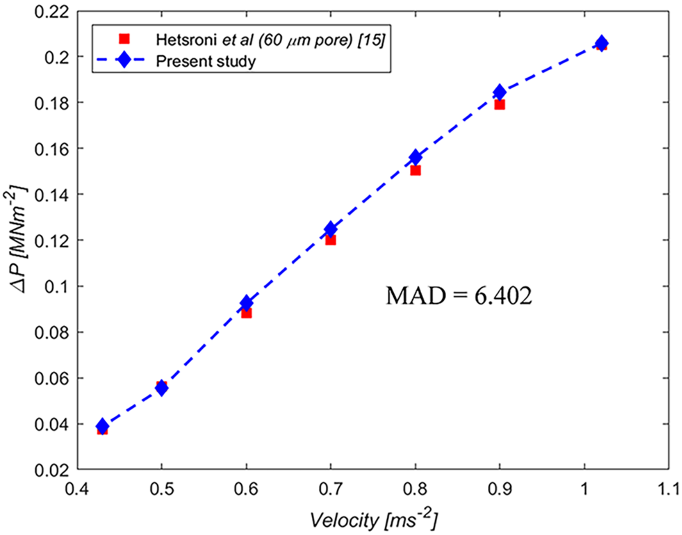

Fig. 6 Comparative analysis of (MCHS without porous medium) Nusselt number in present study versus Kalteh et al. [17]

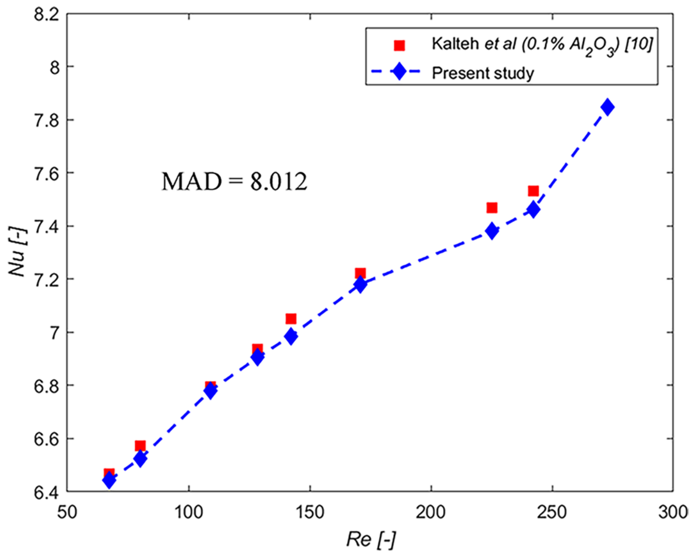

Fig. 7 Comparative analysis of (MCHS with porous medium) pressure drop in present study and Hetsroni et al. [42]

Numerical Model Validation

Experimental data from existing studies are utilized to validate the developed two-phase flow model in Fluent. This validation involves comparisons across various models, including single-phase, two-phase, and sintered porous medium configurations. In the single-phase scenario, water serves as the heat transfer fluid within the microchannel heat sink, comprising solid and fluid regions. A porous substrate is strategically positioned midway toward the outlet, with constant heat flux supplied to the bottom of the heat sink. Comparative analysis is conducted between numerical pressure drop results and experimental observations from Qu and Mudawar [41], as illustrated in Fig. 5.

Evaluation of the two-phase Eulerian-Eulerian model is performed against experimental data from Kalteh et al. [17] for alumina/water nanofluid, specifically focusing on Nusselt number comparison, as depicted in Fig. 6. Both phases enter the microchannel with identical axial velocity, with outlet conditions assumed for both. Strong agreement between numerical simulations and experimental findings is observed. Additionally, the sintered porous medium model undergoes scrutiny against experimental results from Hetsroni et al. [42] concerning pressure drop, as portrayed in Fig. 7. Notably, this experimental setup involves a porous medium characterized by a pore size of 60 µm. The error analysis in this study shows that the mean absolute deviations for the pressure drops are 11.004 and 6.402 while the mean absolute deviation for the Nusselt number is 0.812.

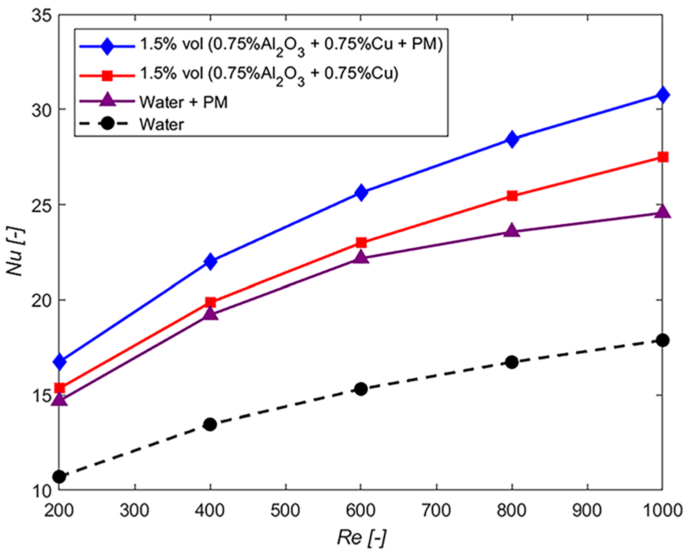

Fig. 8 Comparison of the average Nusselt number at different Reynolds number for water, hybrid nanofluid, water plus porous substrate and hybrid nanofluid plus porous substrate

Table 3 Contours of temperature distribution in the microchannel at Reynolds number of 1 000 for pure water and particle volume concentration of 1.5%

Temperature: No porous substrate	Temperature: With porous substrate
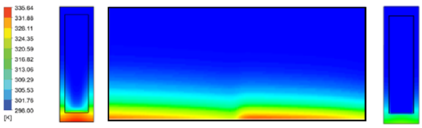 Re 1000, Water	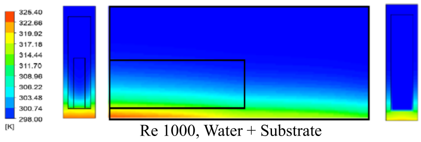 Re 1000, Water + Substrate
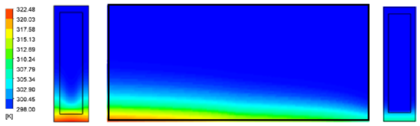 Re 1000, 1.5% vol (0.75%Al_2O_3 0.75% Cu)	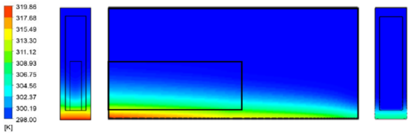 Re 1000, 1.5% vol (0.75%Al_2O_3 0.75% Cu) + Substrate

Results and Discussion

Considering the heat transfer (Nusselt number and thermal resistance) and pressure drop in the defined model with and without porous medium at different nanofluid volume fractions and water as the base fluid at different flows, Reynold numbers ranging from 200 to 1 000. The results are presented and discussed in the sub-sections below.

Influence of Porous Substrate on Average Heat Transfer, Pressure Drop, and Thermal Resistance

The analysis of the average Nusselt number, depicted in Fig. 8, provides insights into the impact of volume concentration and the presence of porous substrate on heat transfer in the microchannel heat sink (MCHS). As depicted, an increase in Reynolds number resulted in a rise in the average Nusselt number. This trend is attributed to the reduction in the thermal boundary layer thickness, allowing higher-velocity fluid to carry more thermal energy and thus enhance heat transfer. However, Fig. 8 further shows that the rate of heat transfer from the heated bottom wall increased with the synergistic interaction between the nanofluid and the porous substrate in the micro channel. This enhancement in heat transfer is visually represented in Table 3. The temperature contour of the microchannel, presented in Table 3 (Mid-plane contour along the flow direction), provides critical insights into the thermal behavior of the system under various flow conditions. Table 3 visually represent the thermal gradients along the microchannel wall. As the fluid flows along the length of the microchannel, the contour plots in Table 3 shows that the case where nanofluid plus porous substrate are employed, particularly at a high Reynolds number of 1 000, is the most effective in reducing the maximum temperature at the heated bottom wall of the micro channel heat sink. This can be attributed to the suspension of hybrid nanoparticles in the base fluid which induced vigorous collisions and increased thermal conductivity of the fluid, further depleting the thermal boundary layer and augmenting heat transfer. Additionally, the integration of

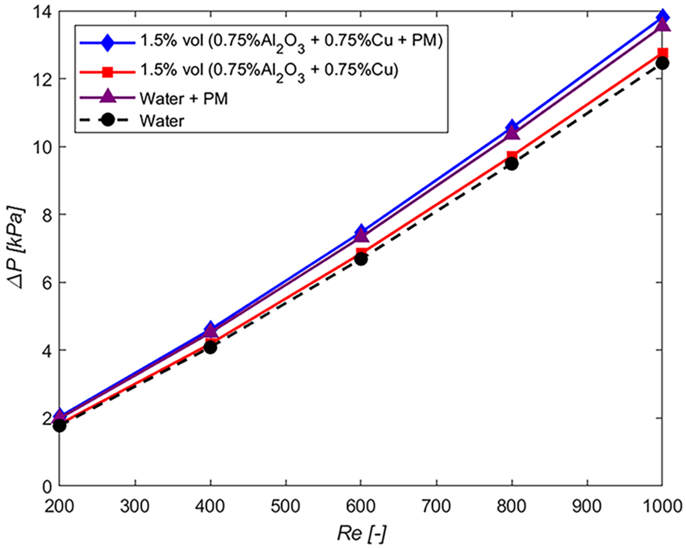

Fig. 9 Comparison of pressure drop in the MCHS at different Reynolds number for water, hybrid nanofluid, water plus porous substrate and hybrid nanofluid plus porous substrate

Table 4 Contours of velocity distribution in the microchannel at Reynolds number of 1 000 for pure water and particle volume concentration of 1.5%

Velocity: No porous substrate	Velocity: With porous substrate
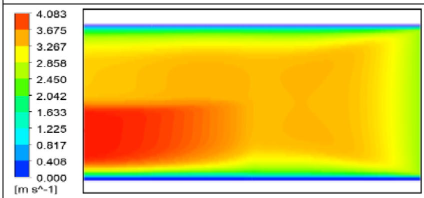 Re 1000, Water	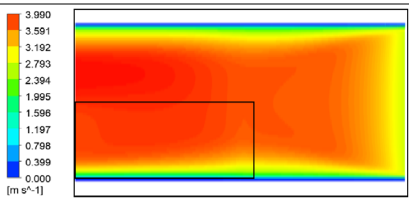 Re 1000, Water + Substrate
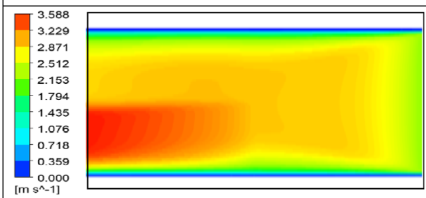 Re 1000, 1.5% vol (0.75%Al_2O_3 0.75% Cu)	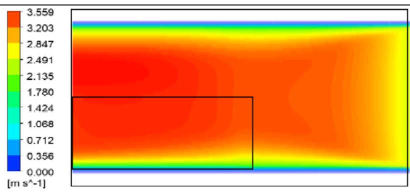 Re 1000, 1.5% vol (0.75%Al_2O_3 0.75% Cu) + Substrate

porous substrate increased the surface area and introduced flow instability in the boundary layer, which enhanced the heat transfer rate of the thermal fluid.

Moving to the analysis of pressure drop, presented in Fig. 9, a general increase is observed as Reynolds number increased. This is because, as Reynolds number increased, the flow

Table 5 Contour of base fluid and nanoparticles distribution in the porous substrate at Reynolds number of 1 000 and for particle volume concentration of 1.5%

Contour of volume fraction

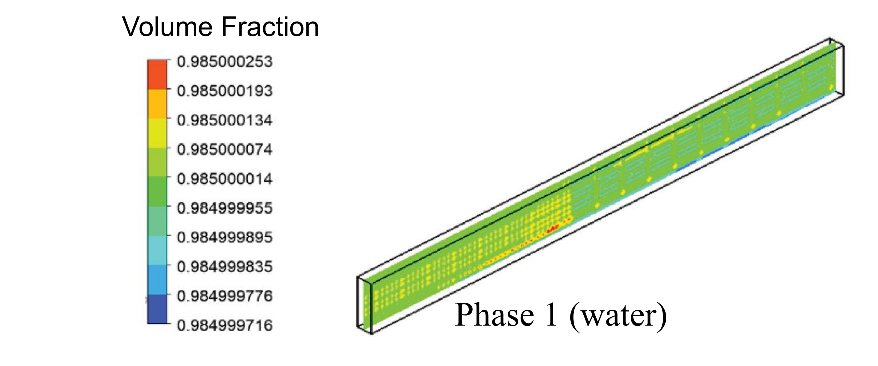

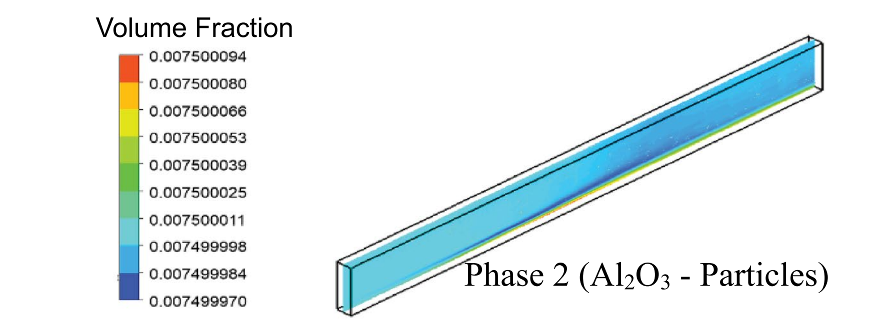

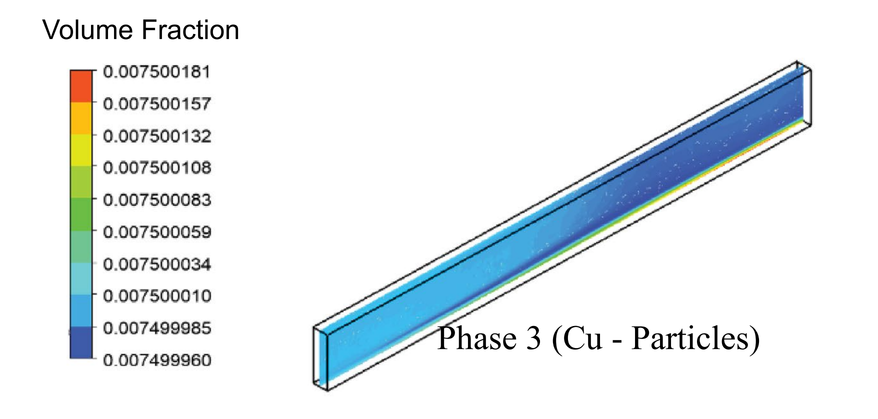

velocity also increased which resulted in greater wall shear stress near the wall of the micro channel. Therefore, the pressure drop which is directly proportional to the shear stress also increased. Figure 9 also compare the pressure drops for the different fluids and flow structure in the micro channel. As seen in Fig. 9, pure water resulted in the lowest pressure drop due to it low dynamic viscosity which led to less internal friction between the fluid layers. Hence lower shear stress against the micro channel wall resulted in lower pressure drop,

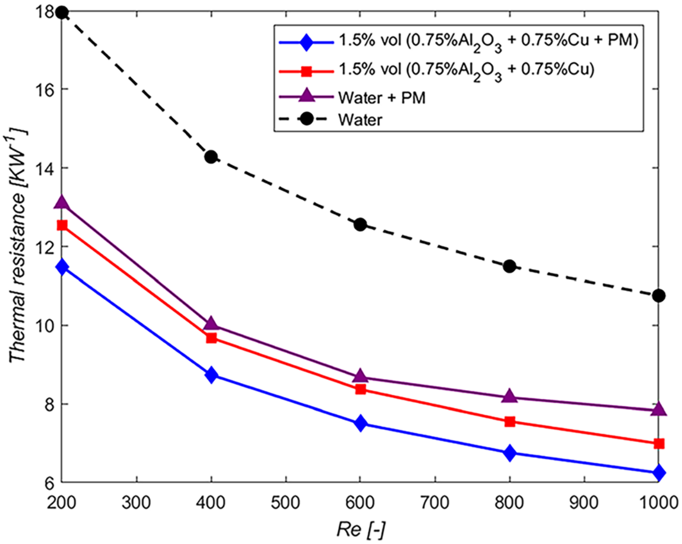

Fig. 10 Comparison of the thermal resistance at different Reynolds number for water, hybrid nanofluid, water plus porous substrate and hybrid nanofluid plus porous substrate

as only the channel wall friction contributes to the pressure drop. However, the addition of nano particle and the presence of porous substrate introduces additional source of resistance to flow in the channel. This is also visually represented in Table 4 (Mid-plane contour along the flow direction). As seen in Table 4, the case of pure water has very low flow resistance and hence higher flow velocity in the channel compared to the case of combined nano fluid and porous substrate. This is because, the nano particles increased the effective viscosity of the fluid which cause viscous drag, while the porous substrate impedes the fluid motion in the microchannel. Therefore, the combined effect of the nano particle and the porous matrix resulted in decreased flow velocity and increased pressure drop within the micro channel. An example of the nano particle distribution in the base fluid (water) for particle volume concentration of 1.5% at Reynolds number of 1 000 is visually represented in Table 5 (Mid-plane contour along the flow direction). The particles slow down and accumulate near the bottom wall of the porous substrate and this is due to the effect of viscous drag and increased flow resistance (lower flow velocity) as shown in Table 4.

Thermal resistance analysis, as shown in Fig. 10, reveals a decrease in thermal resistance with increased Reynolds number. This reduction stems from the depletion in thermal boundary layer thickness as the heat transfer fluid traverses the microchannel. Additionally, the suspension of hybrid nanoparticles increases the thermal conductivity of the heat transfer fluid, leading to a decrease in thermal resistance. Moreover, the integration of porous substrate further resulted in reduced thermal resistance due to the increased surface area available for heat transfer.

In summary, the presence of porous substrate significantly influences heat transfer, pressure drop, and thermal resistance in the microchannel heat sink. The integration of porous substrate enhances heat transfer efficiency while concurrently increasing pressure drop. These findings have important implications for the design and optimization of microchannel heat sinks in various engineering applications.

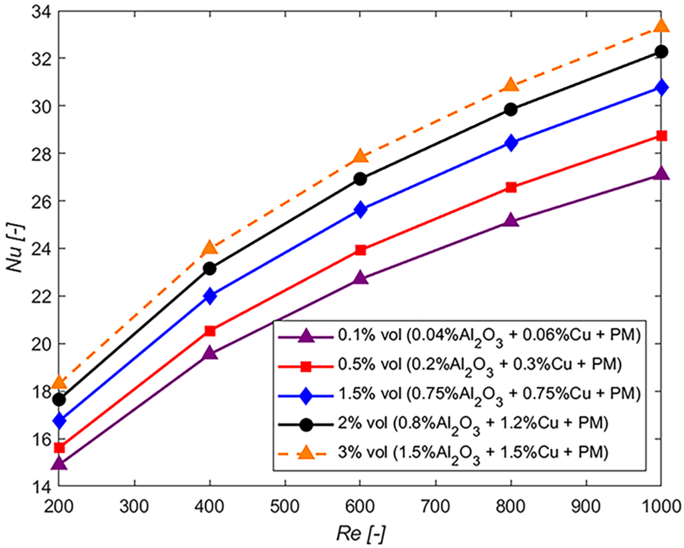

Fig. 11 Impact of nanoparticle volume concentration on the average Nusselt number at different Reynolds number for hybrid nanofluid plus porous substrate configuration

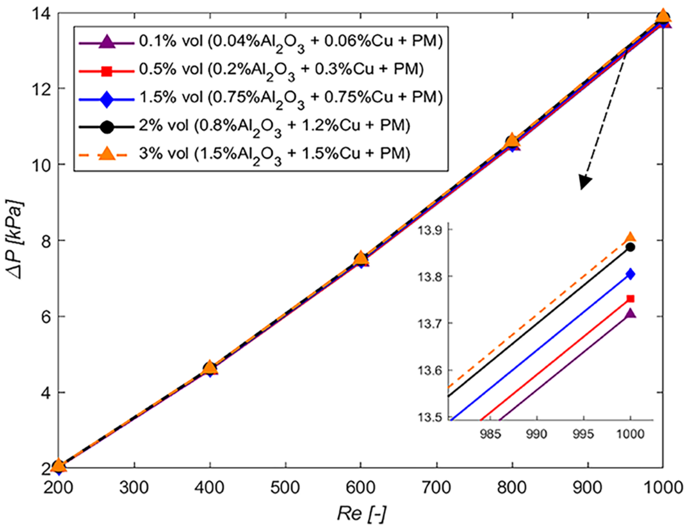

Fig. 12 Impact of nanoparticle volume concentration on pressure drop at different Reynolds number for hybrid nanofluid plus porous substrate configuration

Influence of Nanofluid Concentration on Average Heat Transfer, Pressure Drop, and Thermal Resistance

The analysis of the average Nusselt number in the microchannel heat sink with the presence of porous substrate, considering various volume concentrations (0.1%, 0.5%, 1.5%, 2.0%,

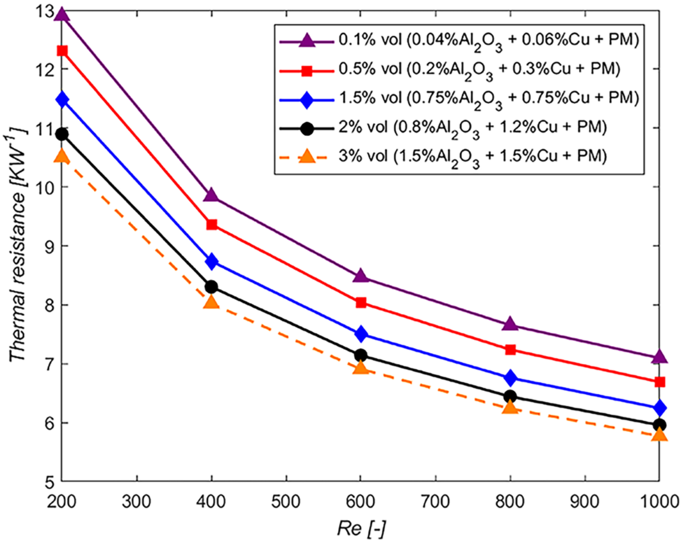

Fig. 13 Impact of nanoparticle volume concentration on thermal resistance at different Reynolds number for hybrid nanofluid plus porous substrate configuration

and 3.0%) of hybrid nanoparticles suspended in the base fluid (water). The results illustrated in Fig. 11 indicate an increase in the average Nusselt number with a rising Reynolds number, further amplified by higher volume concentrations of hybrid nanoparticles. This enhancement is attributed to the thorough mixing of the nanoparticles, resulting in increased thermal conductivity of the fluid and subsequent depletion of the thermal boundary layer. Moreover, the presence of porous substrate contributes to additional depletion of the boundary layer thickness, further enhancing thermal performance.

The pressure drop analysis, depicted in Fig. 12, demonstrates a marginal increase in pressure with increasing Reynolds number as the volume concentration of nanoparticles in the base fluid increased. This increase is primarily due to the heightened inter-collision frequency of nanoparticles at higher velocities, resulting in increased density and resistance to fluid flow. Additionally, the presence of a porous substrate exacerbates the pressure drop by restricting fluid flow further.

The thermal resistance analysis of the microchannel heat sink with porous substrate, considering varying volume concentrations of hybrid nanoparticles, is presented in Fig. 13. The results indicate a reduction in thermal resistance with increasing Reynolds number, further diminished by higher volume concentrations of hybrid nanoparticles. Micro-convection of nanoparticles enhances heat transfer rates, leading to a depletion of the thermal boundary layer and subsequent reduction in thermal resistance. This finding aligns with previous studies by Kumar and Sarkar [43], Eneren et al. [44], Kambli and Dey [45], affirming the inverse relationship between nanofluid volume concentration and thermal resistance. In summary, increasing the volume fraction of hybrid nanofluid enhances thermal performance by augmenting thermal conductivity and depleting the thermal boundary layer thickness. However, this augmentation led to an increase in pressure loss, particularly exacerbated by the presence of a porous substrate.

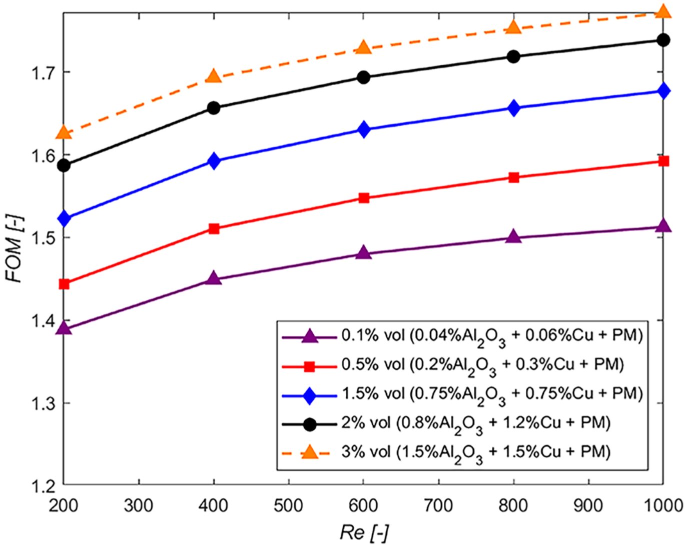

Fig. 14 Variation of figure of merit (FOM) with Reynolds number for different concentrations of the hybrid nanofluids

Figure of Merit

The results shown in Fig. 14 indicate that the Figure of Merit (FOM), which measures the thermal performance of hybrid nanofluids compared to a base fluid, increases with both Reynolds number and nanoparticle concentration. At higher Reynolds numbers, particularly at Reynolds number of 1 000, the flow becomes more turbulent, significantly enhancing convective heat transfer. This is reflected in the maximum FOM (~1.7), observed for the 3% hybrid nanofluid, consisting of 1.5% Al_2O_3 and 1.5% Cu. The improved thermal conductivity of the hybrid nanofluid at this concentration, combined with intensified mixing in turbulent flow, results in a higher heat transfer efficiency compared to lower concentrations and laminar flow conditions.

Conversely, the minimum FOM (~1.4) occurs at the lowest Reynolds number (Re = 200) and at the lowest nanoparticle concentration (0.1% vol.), highlighting reduced thermal conductivity and less efficient heat transfer in laminar flow. This trend emphasizes that hybrid nanofluids are most effective in enhancing heat transfer when used at higher flow rates and particle concentrations. Overall, these findings underscore the importance of both flow dynamics and nanoparticle loading in optimizing the thermal performance of systems using hybrid nanofluids, which demonstrate significant improvements under the right operational conditions.

Conclusion

In conclusion, this research extensively explored the impact of hybrid nanofluid volume concentration and porous substrate integration on microchannel heat sink (MCHS) performance. Utilizing ANSYS Fluent with a two-phase Eulerian-Eulerian approach, our analysis spanned volume concentrations of Al_2O_3/Cu-water hybrid nanofluid from 0.1 to 3.0% as the heat transfer medium. We also assessed the effects of porous substrates positioned halfway towards the outlet of the microchannel heat sink within Reynolds numbers ranging from 200 to 1000, maintaining a fixed heat flux of 1.0 MW/m2. The study findings underscore the substantial influence of hybrid nanofluid volume concentration and Reynolds number on heat transfer coefficient, average Nusselt number, thermal resistance, and pressure loss within the microchannel heat sink. Importantly, porous substrate integration further enhances these parameters, particularly the heat transfer coefficient (i.e. average Nusselt number).

The novelty of this research lies in the simultaneous consideration of dual enhancement techniques, hybrid nanofluids and porous media insertion within a unified two-phase flow framework, which to the best of our knowledge has not been previously modeled in this form. Additionally, the adoption of the Eulerian–Eulerian multiphase model enabled a more accurate representation of interphase heat and momentum exchange between nanoparticles and the base fluid, distinguishing this study from prior single-phase or mixture-based simulations.

Key findings from our investigation include:

i. Influence of hybrid nanofluid volume concentration:

a) Increasing the volume concentration of hybrid nanoparticles resulted in enhanced heat transfer coefficient (i.e. average Nusselt number).

b) Hybrid nanofluid concentration exhibited a moderate effect on pressure drop within the microchannel heat sink.

ii. Impact of Reynolds number:

a) Higher Reynolds numbers correlated with increased heat transfer coefficient and average Nusselt number.
b) Pressure drop showed an increasing trend with higher Reynolds numbers.

iii. Enhancement with porous substrate integration:

a) The integration of porous substrates led to further improvement in heat transfer coefficient.
b) The presence of porous substrates mitigated thermal resistance, contributing to enhanced overall thermal performance.
c) Enhancement heat transfer of 80.29% % was observed with the highest nanofluid volume with the MCHS having a porous medium.

iv. Figure of merit (FOM).

a) The FOM increases with increase in the thermal conductivity of the hybrid nanofluid.
b) The maximum FOM corresponds to Reynolds number of 1 000 at maximum concentration of 3%.
c) The minimum FOM corresponds to Reynolds number of 200 at concentration of 0.1%.

In summary, this study underscores the effectiveness of employing hybrid nanofluids and integrating porous substrates to enhance MCHS performance. Compared to conventional setups using only base fluid as the heat transfer medium, the use of hybrid nanofluids and porous substrates offers improved heat transfer efficiency and overall thermal performance in MCHS applications. These insights provide valuable guidance for optimizing microchannel heat sink design in diverse engineering contexts.

Acknowledgements This research was conducted using the facilities available at the Royal Society Research Lab, University of Lagos, Akoka, Lagos. The support of the facility managers is duly acknowledged and appreciated.

Author Contributions Jeremiah O. Oladetan contributed to the formal analysis, data curation and analysis, visualization and writing of original draft. Faridat M. Fujah was responsible for formal analysis, data curation and analysis, visualization and writing of original draft. Oluwasegun S. Omosehin carried out the conceptualization, methodology, investigation, validation, resource coordination, and drafted the original manuscript. Emmanuel O. Atofarati contributed to the writing of the original draft, project administration, original draft review and editing process, and served as the corresponding author. Uzo Nwabuko supported data curation, visualization, software integration, and assisted with supervision and manuscript review and editing. Olabode T. Olakoyejo contributed to supervision, conceptual design, funding acquisition, and manuscript review and editing. Adekunle O. Adelaja provided technical resources, software support, validation, and contributed to the manuscript's review and editing.

Funding Open access funding provided by University of South Africa.

Data Availability Data will be made available on request.

Declarations

Conflict of Interest The authors declare no conflict of interest.

Open Access This article is licensed under a Creative Commons Attribution 4.0 International License, which permits use, sharing, adaptation, distribution and reproduction in any medium or format, as long as you give appropriate credit to the original author(s) and the source, provide a link to the Creative Commons licence, and indicate if changes were made. The images or other third party material in this article are included in the article's Creative Commons licence, unless indicated otherwise in a credit line to the material. If material is not included in the article's Creative Commons licence and your intended use is not permitted by statutory regulation or exceeds the permitted use, you will need to obtain permission directly from the copyright holder. To view a copy of this licence, visit http://creativecommons.org/licenses/by/4.0/.

References

1. Atofarati, E.O., Sharifpur, M., Meyer, J.: Hydrodynamic effects of hybrid nanofluid jet on the heat transfer augmentation. Case Stud. Therm. Eng. **51**, 103536 (2023). https://doi.org/10.1016/J.CSITE.2023.103536
2. Kumar, A., Lahane, S., Kumar, C.B., Mohan, I., Lata, D.B.: Effect of tri-ethylene glycol mono Methyl ether and alumina additives on ignition delay in a hydrogen fuelled dual-fuel diesel engine. Int. J. Hydrogen Energy. **49**, 1123–1132 (2024). https://doi.org/10.1016/J.IJHYDENE.2023.10.114
3. Galpaya, C., Induranga, A., Vithanage, V., Mantilaka, P., Koswattage, K.R.: Comparative study on the thermal properties of engine oils and their nanofluids incorporating Fullerene-C60, TiO2 and Fe2O3 at different temperatures. Energies. **17**(732) (2024). https://doi.org/10.3390/EN17030732
4. Thesiya, D., Patel, H., Patange, G.S.: A comprehensive review electronic cooling: A nanomaterial perspective. Int. J. Thermofluids. **19**, 100382 (2023). https://doi.org/10.1016/J.IJFT.2023.100382

5. Choi, S.U.S.: Eastman. Enhancing thermal conductivity of fluids with nanoparticles. ASME Int. Mech. Eng. Fluids Eng. Div. FED. **8**(231), 99–105 (1995). https://doi.org/10.1021/je60018a001
6. Nwaokocha, C., Momin, M., Giwa, S., Sharifpur, M., Murshed, S.M.S., Meyer, J.P.: Experimental investigation of thermo-convection behaviour of aqueous binary nanofluids of MgO-ZnO in a square cavity. Therm. Sci. Eng. Prog. **28**, 101057 (2022). https://doi.org/10.1016/J.TSEP.2021.101057
7. Atofarati, E.O., Sharifpur, M., Meyer, J.P.: Pulsating nanofluid-jet impingement cooling and its hydrodynamic effects on heat transfer. Int. J. Therm. Sci. **198**, 108874 (2024). https://doi.org/10.1016/J.IJTHERMALSCI.2023.108874
8. Zhou, J., Cao, X., Zhang, N., Yuan, Y., Zhao, X., Hardy, D.: Micro-Channel heat sink: A review. J. Therm. Sci. **29**(6), 1431–1462 (2019). https://doi.org/10.1007/S11630-020-1334-Y
9. Gupta, S., Subbarao, P.M.V.: Empirical investigation of nanofluid performance in a microchannel heat sink for various attributes in low Reynolds number range. Int. J. Heat. Fluid Flow. **105**, 109258 (2024). https://doi.org/10.1016/J.IJHEATFLUIDFLOW.2023.109258
10. Najafpour, A., Hosseinzadeh, K., Ranjbar Kermani, J., Ranjbar, A.A., Ganji, D.D.: Numerical study on the impact of geometrical parameters and employing ternary hybrid nanofluid on the hydrothermal performance of mini-channel heat sink. J. Mol. Liq. **393**, 123616 (2024). https://doi.org/10.1016/J.MOLLIQ.2023.123616
11. Sheik, M.A., et al.: Study the effect of silicon nanofluid on the heat transfer enhancement of Triangular-Shaped open microchannel heat sinks. Silicon. **16**(1), 277–293 (2024). https://doi.org/10.1007/S12633-023-02663-5/METRICS
12. Jing, D., Song, S., Pan, Y., Wang, X.: Size dependences of hydraulic resistance and heat transfer of fluid flow in elliptical microchannel heat sinks with boundary slip. Int. J. Heat. Mass. Transf. **119**, 647–653 (2018). https://doi.org/10.1016/J.IJHEATMASSTRANSFER.2017.11.149
13. Olakoyejo, O.T., Adelaja, A.O., Adewumi, O.O., Oluwo, A.A., Bello, S.K., Adio, S.A.: Constructal heat transfer and fluid flow enhancement optimization for cylindrical microcooling channels with variable cross-section. Heat. Transf. **50**(7), 6757–6775 (2021). https://doi.org/10.1002/HTJ.22202
14. Olakoyejo, O.T., et al.: Numerical forced convection heat transfer, fluid flow and entropy generation analyses of Al2O3- water nanofluid in elliptical channels. Niger J. Technol. Dev. **19**(4), 361–372 (2022). https://doi.org/10.4314/NJTD.V19I4.9
15. Olakoyejo, O.T., et al.: Computational heat transfer fluid flow analysis in a diamond hole microchannel. FUOYE J. Eng. Technol. (2023). https://doi.org/10.46792/FUOYEJET.V8I1.887
16. Martínez, V.A., Vasco, D.A., García-Herrera, C.M., Ortega-Aguilera, R.: Numerical study of TiO2-based nanofluids flow in microchannel heat sinks: Effect of the Reynolds number and the microchannel height. Appl. Therm. Eng. **161**, 114130 (2019). https://doi.org/10.1016/J.APPLTHERMALENG.2019.114130
17. Kalteh, M., Abbassi, A., Saffar-Avval, M., Frijns, A., Darhuber, A., Harting, J.: Experimental and numerical investigation of nanofluid forced convection inside a wide microchannel heat sink. Appl. Therm. Eng. Vol. **36**(1), 260–268 (2012). https://doi.org/10.1016/J.APPLTHERMALENG.2011.10.023
18. Omosehin, O.S., Adelaja, A.O., Olakoyejo, O.T., Oyekeye, M.O.: Numerical study of the thermal performance and pressure drops of water-based Al2O3 - Cu hybrid nanofluids of different compositions in a microchannel heat sink. Microfluid Nanofluidics. **26**(7), 1–13 (2022). https://doi.org/10.1007/S10404-022-02550-2/FIGURES/10
19. E. H. Rikitu and O. D. Makinde. Mixed Convection of Cu–H2O Nanofluid in a Darcy–Forchheimer Porous Medium Microchannel with Thermal Radiation and Convective Heating. *J. Nanofluids* 2023 12(7):1921–1935. doi: 10.1166/JON.2023.2097
20. Jalili, B., Rezaeian, A., Jalili, P., Ommi, F., Domiri, D., Ganji: Numerical modeling of magnetic field impact on the thermal behavior of a microchannel heat sink. Case Stud. Therm. Eng. **45**, 102944 (2023). https://doi.org/10.1016/J.CSITE.2023.102944
21. Abdollahi, S.A., et al.: Computer simulation of cu: AlOOH/water in a microchannel heat sink using a porous media technique and solved by numerical analysis AGM and FEM. Theor. Appl. Mech. Lett. **13**(3), 100432 (2023). https://doi.org/10.1016/J.TAML.2023.100432
22. Adio, S.A., Alo, T.A., Olagoke, R.O., Olalere, A.E., Veeredhi, V.R.: Ewim. Thermohydraulic and entropy characteristics of Al2O3-water nanofluid in a ribbed interrupted microchannel heat exchanger. Heat. Transf. **50**(3), 1951–1984 (2021). https://doi.org/10.1002/HTJ.21964
23. Farahani, S.D., Alibeigi, M., Zakinia, A., Goodarzi, M.: The effect of microchannel-porous media and nanofluid on temperature and performance of CPV system. J. Therm. Anal. Calorim. **147**(14), 7945–7960 (2022). https://doi.org/10.1007/S10973-021-11087-5/FIGURES/11
24. Farahani, S.D., Farahani, A.D., Hajian, E.: Effect of PCM and porous media/nanofluid on the thermal efficiency of microchannel heat sinks. Int. Commun. Heat. Mass. Transf. **127**, 105546 (2021). https://doi.org/10.1016/J.ICHEATMASSTRANSFER.2021.105546

25. Wang, J., et al.: Simulation of hybrid nanofluid flow within a microchannel heat sink considering porous media analyzing CPU stability. J. Pet. Sci. Eng. **208**, 109734 (2022). https://doi.org/10.1016/J.PETROL.2021.109734
26. Adogbeji, V.O., Atofarati, E.O., Sharifpur, M., Meyer, J.P.: Magnetohydrodynamics of nanofluid internal forced convection: A review and outlook for practical applications. Results Phys. **68**, 108082 (2025). https://doi.org/10.1016/J.RINP.2024.108082
27. Atofarati, E.O., Mebarek-Oudina, F., Huan, Z.: Magnetothermal and magnetorheological nanofluids. In: Simulation Techniques, Biomedical Engineering Applications, and Potential Health Risks, vol. 1, 1st edn. De-Gruyter (2025)
28. Atofarati, E.O., Sharifpur, M., Huan, Z.: Nanofluids for heat transfer enhancement: A holistic analysis of research advances, technological progress and regulations for health and safety. Cogent Eng. (2024). https://doi.org/10.1080/23311916.2024.2434623
29. Rezaei Gorjaei, A., Rahmani, R.: Numerical simulation of nanofluid flow in a channel using Eulerian–Eulerian Two-Phase model. Int. J. Thermophys. **42**(5), 1–16 (May 2021). https://doi.org/10.1007/S10765-021-02821-0/FIGURES/16
30. Bazdidi-Tehrani, F., Ebrahimi, A., Azimi-Souran, R.: Investigation of forced convection of a novel hybrid nanofluid containing NEPCM in a square microchannel: Application of single-phase and Eulerian-Eulerian two-phase models. Numer. Heat. Transf. Part. Appl. (2025). https://doi.org/10.1080/10407782.2024.2305231
31. Olakoyejo, O.T., Adeyemi, E., Adewumi, S.O., Abolarin, S.M., Fetuga, I.A., Adelaja, S.O.: Numerical investigation of Two-Phase Thermal-Hydraulic characteristics and entropy generation of Water-Based Al_2O_3-Cu hybrid nanofluids in microchannel heat sink. ITEGAM-JETIA. **11**(51), 227–235 (2025). https://doi.org/10.5935/JETIA.V11I51.1487
32. Habeeb, A.S., Karamallah, A.A., Aljabair, S.: Review of computational multi-phase approaches of nano-fluids filled systems. Therm. Sci. Eng. Prog. **28**, 101175 (2022). https://doi.org/10.1016/J.TSEP.2021.101175
33. Ali, A.M., Rona, A., Bagdanavicius, A.: Guidance on using two-phase models for predicting the performance of a nanofluid minichannel heat sink. Powder Technol. **452**(120531) (2025). https://doi.org/10.1016/J.POWTEC.2024.120531
34. Salimi, A., Olfati, M., Khoshvaght-Aliabadi, M.: Fluid flow and heat transfer simulations of nanofluids in heat sinks. Nanofluids Prep Appl. Simul. Methods. (2024). https://doi.org/10.1016/B978-0-443-13625-2.00008-5
35. Rowe, P.: Drag forces in a hydraulic model of a fluidised bed-Part II. *Trans. Inst. Chem. Eng.*, (1961). Available: https://cir.nii.ac.jp/crid/1571980074061549568. Accessed 1 Jul 2025
36. Rowe, P.: Drag forces in a hydraulic model of a fluidized bed–part 1. *Trans. Inst. Chem. Eng.*, (1961). Available: https://cir.nii.ac.jp/crid/1370568464637460243. Accessed 1 Jul 2025
37. Wen, C.: Mechanics of fluidization. *Fluid Part. Progress, Chem. Eng.*, [Online]. (1966). Available: https://cir.nii.ac.jp/crid/1572261550060180736. Accessed 1 Jul 2025
38. D. J. Gunn. Transfer of heat or mass to particles in fixed and fluidised beds. Int. J. Heat. Mass. Transf. **21**(4): 467–476. (1978). https://doi.org/10.1016/0017-9310(78)90080-7
39. Schlichting, H., Gersten, K.: Boundary-Layer Theory. Springer Science & Business Media (2003)
40. Nimmagadda, R., Venkatasubbaiah, K.: Two-phase analysis on the conjugate heat transfer performance of microchannel with cu, al, SWCNT, and hybrid nanofluids. J. Therm. Sci. Eng. Appl. (2017). https://doi.org/10.1115/1.4036804/392620
41. Qu, W., Mudawar, I.: Experimental and numerical study of pressure drop and heat transfer in a single-phase micro-channel heat sink. Int. J. Heat. Mass. Transf. **45**(12), 2549–2565 (2002). https://doi.org/10.1016/S0017-9310(01)00337-4
42. Hetsroni, G., Gurevich, M., Rozenblit, R.: Aug. Metal foam heat sink for transmission window. *Int. J. Heat Mass Transf.*, vol. 48, no. 18, pp. 3793–3803, (2005). https://doi.org/10.1016/J.IJHEATMASSTRANSFER.2005.02.040
43. Kumar, V., Sarkar, J.: Effect of different nanoparticle-dispersed nanofluids on hydrothermal-economic performance of minichannel heat sink. J. Therm. Anal. Calorim. **141**(4): 1477–1488. https://doi.org/10.1007/S10973-019-09145-0/FIGURES/16
44. Eneren, P., Aksoy, Y.T.: Vetrano. Experiments on Single-Phase nanofluid heat transfer mechanisms in microchannel heat sinks: A review. Energies. **15**(7), 2525 (2022). https://doi.org/10.3390/EN15072525
45. Kambli, A., Dey, P.: Effects of magnetic fields and nanoparticle concentration on hydro-thermal performance of a surface enhanced microchannel. Numer. Heat. Transf. Part. Appl. (2024). https://doi.org/10.1080/10407782.2024.2373966

Publisher's Note Springer Nature remains neutral with regard to jurisdictional claims in published maps and institutional affiliations.